



Localized Corrosion Behavior of AZ31B Magnesium Alloy with an Electrodeposited Poly(3,4-Ethylenedioxythiophene) Coating

Ushula M. Tefashe,^a Philippe Dauphin-Ducharme,^{a,*} Mohsen Danaie,^b Zachary P. Cano,^c Joseph R. Kish,^{c,**} Gianluigi A. Botton,^b and Janine Mauzeroll^{a,**,z}

^aLaboratory for Electrochemical Reactive Imaging and Detection of Biological Systems, McGill University, Montreal, Québec H3A 0B8, Canada

^bDepartment of Materials Science and Engineering, Brockhouse Institute for Materials Research and Canadian Centre for Electron Microscopy, McMaster University, Hamilton, Ontario L8S 4M1, Canada

^cCentre for Automotive Materials and Corrosion, McMaster University, Hamilton, Ontario L8S 4L7, Canada

Herein we report the characterization of localized corrosion of AZ31B magnesium alloy electrochemically coated with poly(3,4-ethylenedioxythiophene) (PEDOT) from ionic liquid electrolyte. Several scanning probe techniques including high resolution electron microscopy, SVET, SECM amperometric detection of H₂ fluxes, potentiometric SECM detection of local pH and localized potentiodynamic measurements were used to evaluate the microstructure of the coating and its corrosion protectiveness. In order to examine long-term durability of corrosion protection due to the PEDOT coating, these measurements were performed after different immersion times. It was observed that PEDOT coating appears to lose its protective ability after localized coverage of corrosion products. The results of this study provide important information considering the interest in this coating for use in biomedical implants and prior indications of beneficial passivation.

© The Author(s) 2015. Published by ECS. This is an open access article distributed under the terms of the Creative Commons Attribution 4.0 License (CC BY, <http://creativecommons.org/licenses/by/4.0/>), which permits unrestricted reuse of the work in any medium, provided the original work is properly cited. [DOI: 10.1149/2.0601510jes] All rights reserved.

Manuscript submitted February 12, 2015; revised manuscript received July 22, 2015. Published August 4, 2015.

Replacement of heavy alloy components with light-weight materials is of prime concern for automotive and aerospace manufacturers in order to reduce the fuel consumption and hence polluting CO₂ emissions. Magnesium alloys are one of the potential candidates owing to their excellent physical and mechanical properties such as lower density, a higher strength-to-mass ratio and a higher vibrational damping capacity compared to steel and aluminum alloys.¹ However, the high corrosion susceptibility is the major drawback preventing more widespread use of such Mg-based alloys.

The addition of alloying elements, alternate processing technologies and surface coatings are effective in improving the corrosion performance of Mg-based alloys.^{2,3} Dip coating is particularly attractive to the automotive industry because of its simplicity, low costs and great coverage ability.^{4,5} Coating processes vary from the widely used chromate/manganese dip treatment to anodic treatments in fluoride-containing baths,^{6,7} and are generally considered hazardous to human health and to the environment.^{2,3} More environmentally sustainable surface modification processes were identified in conductive polymers but remain challenging to implement with light metal alloys.^{8,9}

Conducting polymer films are readily formed by direct electrodeposition onto Pt and Au.¹⁰ They have been used for corrosion protection of structural metal like steel and aluminum with success but comprehensive investigations for magnesium materials is lacking. The deposition of conductive polymers onto Mg-based electrodes from aqueous solutions is generally not feasible because the positive potentials required for electropolymerization concurrently form thick surface oxide films and lead to copious hydrogen evolution^{11,12} that prevent the formation of adherent and continuous conducting polymer films.¹³

Room temperature ionic liquids (RTIL's) are increasingly being applied in electrochemistry¹⁴ and have recently been explored as solvents for the electropolymerization of conducting polymers.¹⁵⁻¹⁷ Generally, conducting polymers prepared from ionic liquid solutions have enhanced electrochemically stability¹⁶ compared to their counterparts formed from aqueous solutions. Recently, the electrodeposition of conducting polymer coatings (such as PEDOT) on Mg alloys from the RTIL electrolyte (such as 1-ethyl-3-methylimidazolium bis(trifluoroethylsulfonyl)imide (EMI⁺TFSI⁻)) has been studied for use in biomedical implants.¹⁸ It has been reported that the TFSI⁻

anion of the RTIL leads to the passivation of Mg alloys,¹⁹ while PEDOT displays high chemical and mechanical stability compared to other polymers.^{20,21} Although the PEDOT coating from RTIL has been successfully deposited on a Mg alloy surface previously using an electrochemical method,¹⁸ their corrosion performance is sparsely reported.^{18,22} These previous studies reported that PEDOT coated Mg samples exhibited slower degradation rates compared to that of uncoated samples.

In the present study, we evaluate the corrosion protection of PEDOT coating on AZ31B Mg alloy from RTIL electrolyte containing EDOT monomer and EMI⁺TFSI⁻ electrolyte. To synthesize the PEDOT coating on AZ31B, cyclic voltammetry is used based on an established protocol producing uniform coatings on aluminum alloys and steel.^{23,24} The microstructure of the PEDOT coating was examined using analytical transmission electron microscopy (TEM) on samples prepared via the focused ion beam (FIB) in-situ lift-out technique. The corrosion behaviour of the coated versus uncoated AZ31B was investigated using localized potentiodynamic polarization (PDP), corrosion potential transients, the scanning vibrating electrode technique (SVET),^{25,26} and scanning electrochemical microscopy (SECM)^{27,28} in 0.01 M NaCl solution with variable immersion times.

Experimental

Materials and sample preparation.— The samples for this study were prepared from commercial AZ31B magnesium alloy sheet product received from General Motors in the as-cast condition and machined into 1 cm × 1 cm × 0.7 cm samples. 3,4-ethylenedioxythiophene (EDOT) and 1-ethyl-3-methylimidazolium bis(trifluoro-methylsulfonyl) imide (EMI⁺TFSI⁻, room temperature ionic liquid, electrochemical grade, 99.5% purity) were purchased from Sigma-Aldrich. The chemical structures of electrolyte, EDOT and PEDOT were given in Supporting Information, Figure SI-1. An aqueous NaCl (ACP, Montreal, QC) solution was made with analytical grade reagent and deionized water (Millipore MiliQ water 18.2 MΩ). Micropipette probes were fabricated from a borosilicate glass capillary with an outer to inner diameter ratio of 1.5 mm to 0.7 mm and was pulled to a tip with a diameter of ~1 μm, using a P-2000 CO₂ laser puller (Sutter Instrument). The Pt microelectrodes (Pt ME) were prepared by heat sealing a 12.5 μm radius Pt wire in a borosilicate glass capillary under vacuum followed by further processing to produce the SECM tips, as described previously.²⁹ The aqueous solution for the fabrication of the iridium oxide-coated Pt ME (Pt/IrO_x) sensor

*Electrochemical Society Student Member.

**Electrochemical Society Active Member.

^zE-mail: Janine.mauzeroll@mcgill.ca

comprised a mixture of 75 mg of IrCl_4 , 0.5 mL aliquot of aqueous 30% H_2O_2 , 250 mg of hydrated oxalic acid ($\text{C}_2\text{H}_2\text{O}_4 \cdot 2\text{H}_2\text{O}$) and K_2CO_3 (Sigma-Aldrich). The pH microprobes were fabricated following the method described previously.³⁰ Briefly, a constant current density of 1.5 mA/cm^2 was applied for 3 minutes in galvanostatic mode. Immediately after deposition, the Pt/IrO_x ME was rinsed with distilled water and dried under a stream of nitrogen, and then placed in a pH 7 universal buffer for 24 hours, a practice which proved to be necessary in order to reduce potential drifts.³⁰ The response time of the probe was measured to be 1 second.³¹ The details of the method are provided in the supplemental information, Figure SI-2.

Instrumentations and procedures.— Electrochemical deposition of PEDOT onto one half of the AZ31B alloy surface (while masking the other half of the surface with tape) was performed using cyclic voltammetry (CV) in a three-electrode setup with the AZ31B alloy acting as the working electrode, a coiled platinum wire (0.5 mm diameter) as the counter electrode and a chloridized silver wire (1.0 mm diameter) as the quasi-reference electrode (Ag/AgCl-QRE). The electrochemical cell was made from polytetrafluoroethylene (PTFE) with an opening at the center into which the epoxy-mounted AZ31B alloy working electrode was tightly fitted.³² The working electrode was polished and cleaned prior to the electrodeposition experiment according to a previously established procedure.^{32,33} The electrolyte bath for the electrochemical deposition was prepared by mixing EDOT and $\text{EMI}^+\text{TFSI}^-$ to give a 0.1 M EDOT concentration. The electrodeposition by the CV method involved cycling the potential between -2.0 and $+2 \text{ V}$ vs Ag/AgCl-QRE for 30 cycles with a scan rate of 100 mV/s to achieve compact and adherent PEDOT films on the substrate. The potential scan was stopped at -2.0 V such that the PEDOT film was in its reduced, low conductivity state. PEDOT film formation using CV produced more uniform films than potentiostatic PEDOT deposition. The incomplete reduction of PEDOT inherent in potentiostatic deposition could lead to the accumulation of residual oxidized PEDOT species in the film, which could cause the degradation of the polymer film.

In order to characterize the surface microstructure after the deposition of the PEDOT layer, we performed analytical TEM on samples prepared via the FIB in-situ lift-out technique. Two locations were selected for FIB sample preparation, one entirely within the coated region and the other at the boundary between coated and uncoated areas. A Zeiss NVision 40 dual beam (SEM/FIB) system was used for FIB preparation. TEM analysis was performed on an FEI Titan 80–300 (S)TEM equipped with an X-ray energy dispersive spectrometer (XEDS- Oxford, Inca, Si(Li) detector). All TEM measurements were performed while the sample temperature was maintained at 95 K to minimize electron beam induced damage.

For micropipette-based PDP measurements, a small microcapillary probe with a tip diameter of about $1 \mu\text{m}$ was filled with a 0.01 M NaCl electrolyte solution. The liquid meniscus of the electrolyte solution protruding from the end of the pipet was brought into gentle contact with the substrate, where it was held by surface tension. The filled capillary was connected to a Ag/AgCl-QRE wire reference-counter electrode, while the wetted area of the substrate defined the working electrode, thereby forming a conventional two electrode electrochemical cell, and, consequently, a series of PDP curves were measured. To allow easy positioning of the probe on the sample, the micropipette was attached to the SECM positioning stage.

SVET measurements were performed using a Princeton Applied Research Model 370 Scanning Electrochemical Workstation. The SVET involves the vibration of a Pt electrode tip (in a direction normal to the electrode surface) whilst measuring the voltage difference between the two extremes of the tip's position. The voltages of the Pt tip (diameter between $5\text{--}50 \mu\text{m}$ as specified by the manufacturer) were measured against a graphite auxiliary electrode. Current density values were extracted from the voltage difference measurements using a calibration equation empirically derived from vibrating electrode measurements of a series of known current densities applied to a gold electrode (following a similar procedure outlined by Williams et al.³⁴)

The Pt tip was positioned approximately $100 \mu\text{m}$ above the AZ31B surface of interest and scanned across a $6 \text{ mm} \times 6 \text{ mm}$ area such that the interface between the PEDOT-coated half and uncoated half ran across the centre of the scan area. SVET scans were completed once every 30 min throughout a 24 hour immersion period in 0.01 M NaCl. The probe outputs were measured using a series of sweeping line scans across the scan area with a speed of $200 \mu\text{m/s}$ and one data point collected every $150 \mu\text{m}$. The probe was vibrated in the vertical direction with an amplitude of $30 \mu\text{m}$ and a frequency of 80 Hz. The gain of the electrometer was set to 10^4 , and the full scale sensitivity of the lock-in amplifier was set to $160 \mu\text{V}$. A schematic representation of the SVET electrode setup is presented in Supporting Information Figure SI-3.

SECM measurements were performed using an ElProScan 3 system (bipotentiostat model PG340, HEKA Electronics, Germany). The SECM apparatus and procedures were described previously.^{29,32} In amperometric substrate generation/tip collection (SG/TC) mode of the SECM, the Pt ME is positioned $10 \mu\text{m}$ above the surface of the Mg alloy electrode, while the ME potential is held at -0.05 V vs Ag/AgCl-QRE such that H_2 evolved from the Mg electrode was oxidized at its tip. The ME current is a measure of the rate of local H_2 evolution, and by scanning the ME at the interface between uncoated and PEDOT-coated AZ31B electrode, an SECM map of H_2 evolution activity can be generated. For pH imaging, the variations in the open circuit potential of Pt/IrO_x microprobe was measured using a constant-height SECM in the potentiometric mode. The Pt/IrO_x microprobes were calibrated before and after each SECM experiment by the sequence of buffer solutions (pH: 1.02, 1.98, 3.51, 5.76, 7.21, 8.03, 10.30 and 12.10). The calibration curve was used to convert the open circuit potential values to pH. In all experiments, an electrolyte concentration of 0.01 M NaCl aqueous solution was used. SVET and SECM measurements were carried out on a coated alloy, while potentiodynamic studies were performed on individual alloys.

Results

Electrodeposition of PEDOT onto AZ31B.— The electrochemical behaviour of Mg alloy AZ31B during successive potential scan between -2 V to $+2 \text{ V}$ vs Ag/AgCl-QRE, at a scan rate of 100 mV/s in 0.01 M $\text{EMI}^+\text{TFSI}^-$ solution without EDOT monomer was examined (Figure 1a). The voltammograms presented an anodic wave ($+0.45 \text{ V}$ vs Ag/AgCl-QRE), assigned to the oxidation of the alloy.

During the electrodeposition of PEDOT from 0.1 M EDOT in 0.01 M $\text{EMI}^+\text{TFSI}^-$ solution at the AZ31B electrode, an onset for the oxidation of the EDOT monomer is apparent at $+0.25 \text{ V}$ with a peak current at $+0.45 \text{ V}$ during the forward scan of 1st CV in Figure 1b. The crossover observed in the 1st CV is characteristic of electrode surface modification related herein to PEDOT polymer formation through a nucleation and growth mechanism.³⁵ In subsequent cycles, the anodic wave observed in Figure 1a without EDOT remained present but the magnitude of the peak current is increased by a 100 fold, consistent with polymer film growth. Continuous CV scans of PEDOT electrodeposition on AZ31B surface for 30 cycles was found to be optimal to obtain a visibly smooth, dark-green PEDOT film. In contrast with electrodeposition from aqueous solutions onto noble metal electrodes,¹⁰ where the current typically increases with deposition cycle, the CVs obtained during electrodeposition in $\text{EMI}^+\text{TFSI}^-$ decreased. This could be due to several factors, such as lower EDOT diffusion to the electrode surface in the viscous ionic liquid, a higher resistance between the substrate and the surface or in the polymer due to interphase layers or differences in the polymer structure and composition.

The mechanism of EDOT electropolymerization (Figure 1c) is expected to be similar to the electropolymerization process of other conducting polymers on electrode surfaces.^{36,37} The initiation step involves the anodic oxidation of EDOT monomers to radical cations in the vicinity of the AZ31B electrode. The radical cations form a dimer that undergoes deprotonation prior to its reoxidation and subsequent reaction with another radical cation. The process continues until the

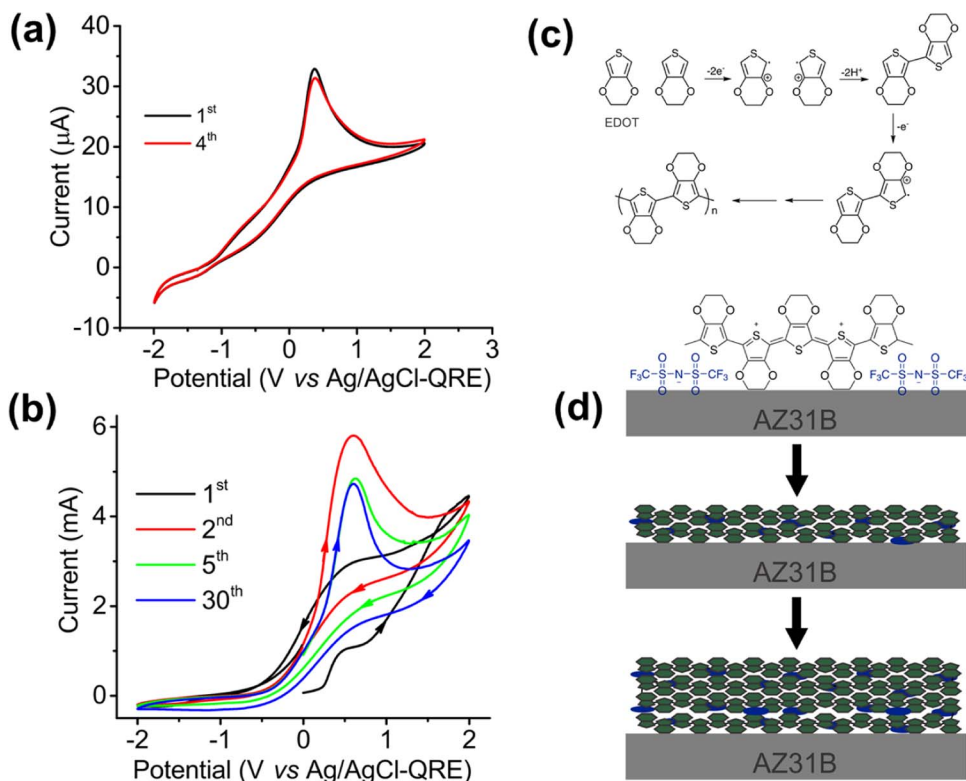


Figure 1. (a) Cyclic voltammetric behavior of AZ31B Mg alloy electrode in an ionic liquid solution of 0.01 M EMI⁺TFSI⁻. (b) Current-potential curves during the cyclic voltammetric deposition of PEDOT from 0.1 M EDOT in 0.01 M EMI⁺TFSI⁻ solution at a 0.5 cm² AZ31B electrode. The potential sweep was from -2 V to +2 V vs Ag/AgCl-QRE at a scan rate of 100 mV/s and was initiated at 0 V vs Ag/AgCl-QRE. (c) Electropolymerization mechanism of EDOT. (d) Possible layering of PEDOT on on AZ31B Mg alloy surface.

chain length of the oligomers exceeds the solubility limit of the solvent and precipitates onto the AZ31B electrode (Figure 1d). The film continues to grow as more polymer is formed by the continued transport of electrons from the conductive-polymer electrolyte surface.

Surface characterization of the PEDOT-coated AZ31B.— PEDOT polymer film deposition was confirmed using IR (Figure SI-4). Consistent with previous report³⁸ the peaks near 830 and 933 cm⁻¹ correspond to the vibrations of S-C bonds in polymerized PEDOT chains. The strong peak at 1722 cm⁻¹ is usually associated with the doped state of PEDOT.

To characterize the surface microstructure of the PEDOT-coated region, FIB specimens were prepared. In Figure 2, a representative specimen a fully coated region (*Sample #1*), and a second representative specimen the interfacial region between the coated and uncoated areas (*Sample #2*) are discussed. The frames in panels (a) and (b) in Figure 2 show the locations where the two samples were extracted from, with the final FIB samples imaged by TEM in panels (c) and (d), respectively. The white layer on top of the two samples is the protective W layer deposited during FIB preparation. The PEDOT layer is a porous interlayer between the base AZ31B alloy and the top protective W layer. It can immediately be observed that in *Sample #1* large Al-Mn particles, around 4 µm in diameter, (see Figure 2a and supplementary Figure SI-5) protruded with respect to the coated surface. The vertical distance between the top of the particle and the underlying alloy surface was approximately 1.4 µm, Figure 2c. At the interface area, *Sample #2*, the coated interface was situated lower than the uncoated interface (referring to the provided guidelines), which demonstrated that the PEDOT deposition process involved a recession of the alloy surface, Figure 2d. In areas away from the bare AZ31B/PEDOT-coated interface, the PEDOT thickness can vary between 400–600 nm. This divergence at the maximum point, toward the extreme right side of *Sample #2* in panel (d), was approximately

1.2 µm. The gradual shift in the level of recession in the vicinity of the coated/non-coated interface is possibly due to the coating solution having penetrated underneath the tape to an extent.

A closer view of the PEDOT coating, Figure 3, shows that this layer is highly porous with striations present parallel to the alloy surface, presumably due to the successive deposition of layers. Panel (a) shows the TEM-Bright-Field (BF) micrograph of the PEDOT coating. Panel (b) is a higher magnification TEM-BF image of the PEDOT layer, with the electron diffraction pattern from the same area shown in panel (c). The diffraction pattern is comprised of three highly diffused diffraction rings, and an apparently random distribution of diffraction spots. Experimental diffraction data on deposited PEDOT layers from RTIL's are sparse in the literature. Nevertheless, our observation does not agree with a similarly grown PEDOT layer, reported by Ahmad et al.,³⁹ where they report deposition of crystalline nano-fibers. We did not observe any beam-induced degradation, neither in the image nor in diffraction (as mentioned in the Experimental section, the sample was kept at 95 K), while examining the PEDOT layer using TEM in our experimental cryogenic conditions. The circle in panel (c) shows the location of the objective lens aperture (OLA) for the dark-field (DF) micrograph shown in panel (d). The PEDOT is uniformly illuminated in the DF (except for the pores) with small particles also appearing bright. The composition corresponding to data point #1 in Figure SI-5 is the following: Al 73.89 at.% Mn 21.59 at.% F 4.52 at.%

We also acquired low-loss electron energy EEL spectra from a similar region in *Sample #1* (Figure 4). The frame in the scanning transmission electron microscopy (STEM)-high-angle annular dark-field imaging (HAADF) image in panel (a) shows the region selected for spectrum imaging. Panel (b) is the HAADF signal gathered simultaneously, and with the same pixel size, as the spectrum image. The energy-filtered intensity maps from various portions of the EEL spectra are presented in panels (c) through (f), with representative spectra from marked locations in panel (g). There is a peak at 5.5 eV

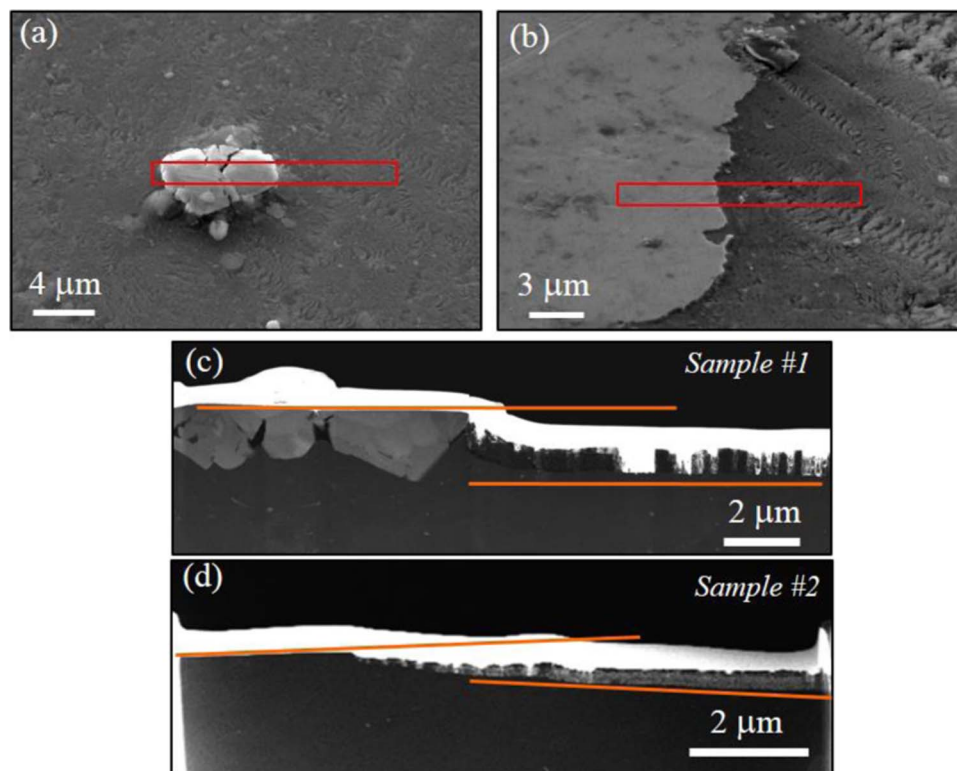


Figure 2. SEM micrographs of (a) an area of the AZ31B sample coated with PEDOT (*Sample #1*), and (b) the interface region of the coated and uncoated areas (*Sample #2*). The areas marked in panels (a) and (b) show the locations selected for the preparation of the FIB samples. (c) and (d) Scanning transmission electron microscopy (STEM)-high-angle annular dark-field imaging (HAADF) micrographs of the FIB samples corresponding to areas shown in (a) and (b), respectively. The images are plan-view SEM micrographs. The orange lines in panels (c) and (d) are simple reference guides to the eye to mark the original surface or the alloy surface following PEDOT deposition.

associated with the alloy/PEDOT interface. The origin of this peak is currently unknown, but could be correlated to surface Zn enrichment (detected by XEDS, Supplementary Figure SI-6, and previously observed in similarly corroded alloy systems.^{40,41}) The intensity map corresponding to ~ 17 eV, Figure 4c, highlights the Al-Mn particles (this value for E_p of Al_8Mn_5 phase was previously reported³³). It is observed that these particles are scattered both within the alloy and within the PEDOT coating, Figure 4e. The size distribution of these particles observed here is comparable to the ones observed in the DF micrograph in Figure 4b. XEDS confirmed that these particles are indeed of Al-Mn type: the results of which are presented in the Supplementary Figure SI-6. EEL spectra #4 (inside the PEDOT coating, green curve in Figure 5g) shows a broad peak centered around 22 eV. XEDS data from the PEDOT layer (Supplementary Figure SI-6) shows that this layer contains C, O, Mg, Al, Si, S, and Cl. Of these elements, C, O, and S belong to the chemical structure of PEDOT. The Mg and Al signal confirms our earlier observation regarding the receding alloy surface. The C signal intensity is surprisingly low given that this layer is essentially a polymer.

Evaluating the corrosion properties of AZ31B-coated with PEDOT.—PDP measurements.—Micropipette-based PDP curves of the uncoated and PEDOT-coated AZ31B alloy were measured after 30 minutes and 24 hours contact of the sample with 0.01 M NaCl solution (contact area of $2.16 \mu\text{m}^2$). The schematic of micropipette-based PDP measurements is described in the Experimental section and is shown in Figure 5a. The PDP curves were measured at least ten times in a given area and the representative PDP curves are displayed in Figure 5b.

Figure 5b reveals the responses of uncoated AZ31B (after 30 minutes (1) and 24 hours (2) of immersion) and PEDOT-coated AZ31B (after 30 minutes (3) and 24 hours (4) of immersion). The 30 min-

utes and 24 hours immersion times herein correspond to the amount of time the drop was in contact with the substrate. Overall, there is a marked reduction in corrosion current density i_{corr} for PEDOT-coated AZ31B ($i_{\text{corr}} = (3.6 \pm 0.4) \times 10^{-6}$ A/cm² after 30 minutes and after 24 hours) compared to that of uncoated AZ31B ($i_{\text{corr}} = 0.8 \pm 0.2$ A/cm² after 30 minutes and $(1.4 \pm 0.8) \times 10^{-2}$ A/cm² after 24 hours). The cathode reaction on the PEDOT-coated surface is under mass transport control. Therefore, the i_{corr} remained the same after 24 hours for the PEDOT-coated AZ31B implies that the limiting current density has been attained. It can also be seen that a shift in corrosion potential (E_{corr}) to more positive values for PEDOT-coated AZ31B ($E_{\text{corr}} = -0.9 \pm 0.2$ V after 30 minutes and -0.3 ± 0.1 V after 24 hours immersion) compared to that of uncoated AZ31B ($E_{\text{corr}} = -1.5 \pm 0.1$ V after 30 minutes and -1.4 ± 0.2 V after 24 hours immersion). By comparing curve 1 to curve 3, and curve 2 to curve 4, it seems like the PEDOT coating drastically reduces the anodic and cathodic reaction rates, relative to corrosion current. The decrease in anodic and cathodic reaction rate for PEDOT coated sample may be due to the PEDOT acting as a physical barrier impeding mass transport of Mg^{+2} ions, as discussed later.

On the other hand, the increase in cathodic reaction rate of PEDOT coated sample after 24 hours immersion compared to 30 minutes immersion may be attributed to: (i) the fact that the Mg alloy surface naturally becomes more cathodically active during corrosion,^{41,42} (ii) the increase in the pH which lead to precipitation of a more protective $\text{Mg}(\text{OH})_2$ layer (see below), and (iii) the increased immersion time allowed further penetration of the electrolyte through the pores in the PEDOT coating, and thus increased the ability of Al-Mn particles to sustain the H_2 evolution reaction. This could explain why the E_{corr} shift was much more dramatic for the PEDOT coating, since the uncoated AZ31B has a much thinner surface film, and thus a smaller number of Al-Mn particles embedded available in a given surface area.

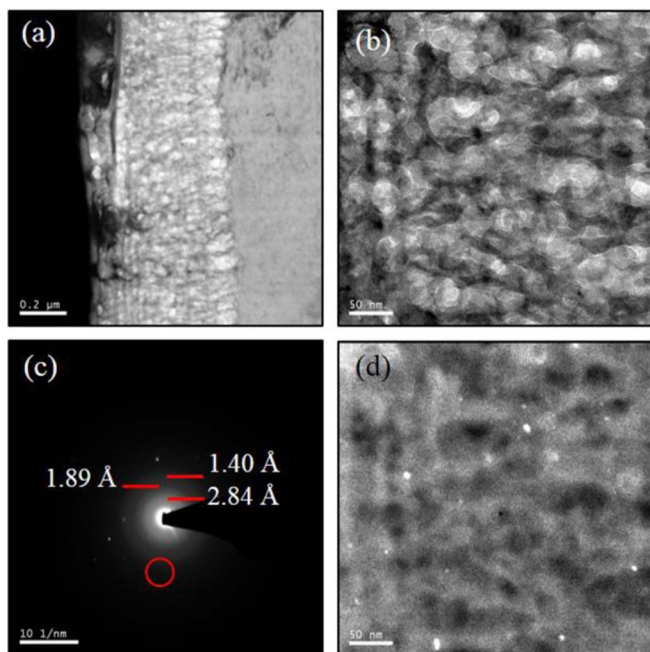


Figure 3. (a) Low magnification TEM-BF micrograph showing the PEDOT layer. (b) TEM-BF micrograph of the PEDOT layer at a higher magnification. (c) Electron diffraction pattern from the area imaged in panel (b). (d) DF micrograph corresponding to the OLA position marked in panel (c).

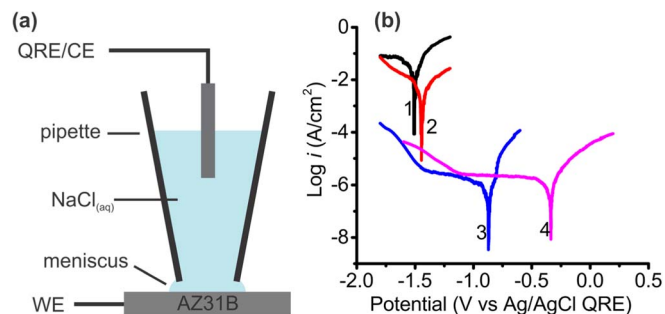


Figure 5. (a) Schematic illustration of the micropipette based technique. The capillary containing 0.01 M NaCl electrolyte solution and Ag/AgCl-QRE quasi-reference/counter electrode has to be lifted from the surface and repositioned after each measurement. (b) Representative PDP curves for the uncoated AZ31B (after 30 minutes (1), after 24 hours (2)) and PEDOT-coated AZ31B (after 30 minutes (3), after 24 hours (4)).

It should be noted here that the cathodic and anodic reaction rates measured on the PEDOT-coated surface may have only originated from defects in the coating, as opposed to uniformly across the entire meniscus contact area. Therefore the measured current densities may not be an accurate representation of the bulk reaction rates on the PEDOT-coated surface.

To determine at which point in time the surface passivity breakdown occurred on the PEDOT-coated AZ31B sample, we measured the E_{corr} transients of the isolated coated and uncoated surfaces (Figure SI-7). It has been reported that the Mg passivity breakdown can be identified by local maximum in the E_{corr} transients.^{34,43} The E_{corr}

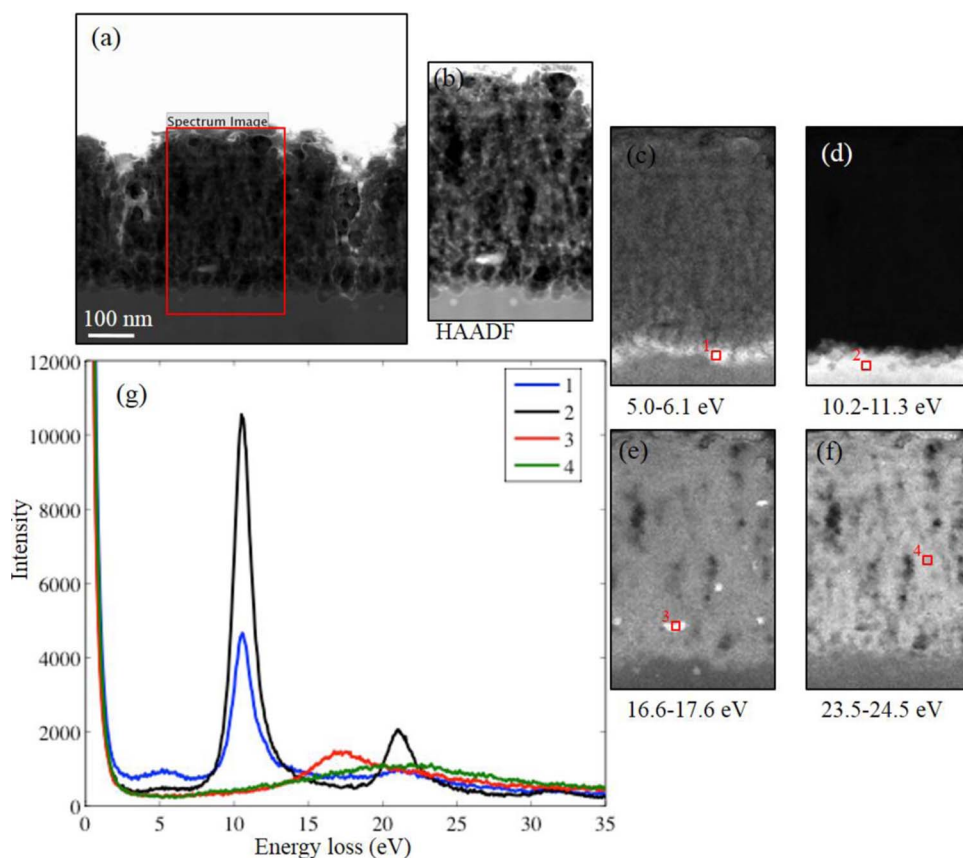


Figure 4. (a) STEM-HAADF image of the PEDOT layer in Sample #1. The area marked was used for low-loss EELS imaging. (b) HAADF signal with the pixel size selected for SI-7. (c)-(f) energy-filtered intensity maps of various energy ranges of the low-loss EEL spectra. (g) Representative EEL spectra from marked regions of the surface layer.

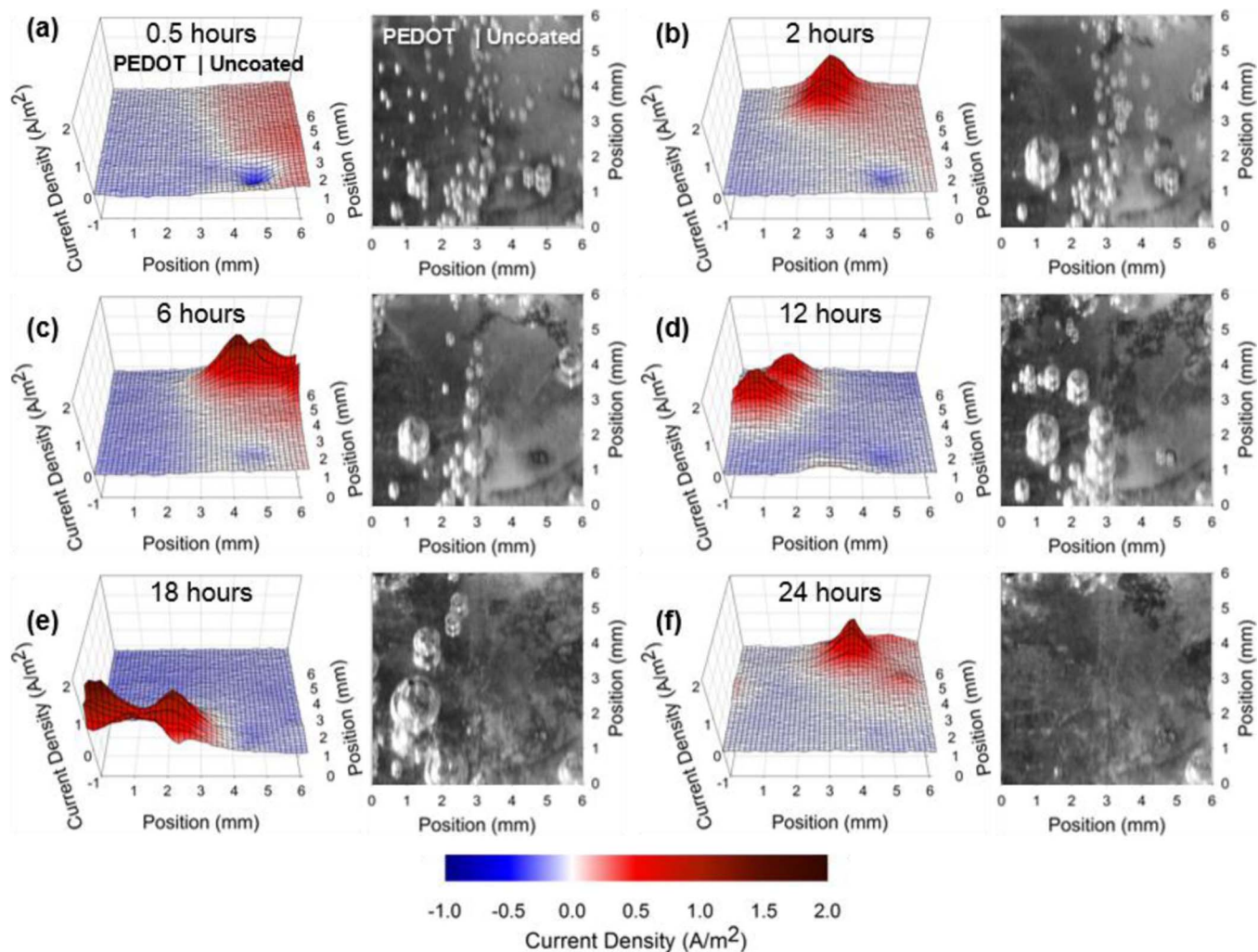


Figure 6. SVET plots and scan area images of the AZ31B sample at various times after immersion in 0.01 M NaCl solution. In each of the plots and scan area image, the PEDOT-coated side is located on the left half and the uncoated side is located on the right half.

transient for the uncoated AZ31B readily shows the onset of the film breakdown (local maxima observed at about 2 hrs, Figure SI-7), but the E_{corr} transient for the PEDOT-coated AZ31B does not show an obvious breakdown point in 24 hour immersion experiments.

SVET measurements.—Representative SVET plots recorded during immersion of the AZ31B sample in 0.01 M NaCl solution are presented in Figure 6. Corresponding images of the scan area are also provided alongside the SVET plots. In each of the plots and scan area images, the PEDOT-coated side is located on the left half and the uncoated side is located on the right half. In the first SVET scan (completed after 30 minutes of immersion), cathodic currents were predominantly observed on the PEDOT-coated half while anodic currents were predominantly observed on the uncoated half (Figure 6a). This result is expected based on the PDP curves presented in Figure 5b, since the E_{corr} difference between the uncoated and PEDOT-coated. The cathodic current densities were uniform across the entire PEDOT-coated half with an average value of -0.1 A/m^2 . On the uncoated half of the alloy, the detected anodic currents became larger as the probe moved further away from the interface between the PEDOT-coated and uncoated sides. The maximum anodic current density was 0.3 A/m^2 . A relatively intense local cathode with a peak current density of -0.5 A/m^2 was also observed on the uncoated half of the specimen, which may have corresponded to a large Al-Mn or Al-Mn-Zn particle.¹¹

Localized corrosion was initiated after approximately 2 hours of immersion (Figure 6b). While the first corrosion locations initiated

on the uncoated half, it propagated such that corrosion regions were soon observed on both the PEDOT-coated and uncoated sides (Figures 6b,6c). Intense local anodes with peak current densities of up to 2 A/m^2 were detected (Figures 6b–6f), which is consistent with previous observations.⁴² After 12 hours, moderate cathodic currents (average current density of -0.1 A/m^2) were observed in the wake of the corrosion regions on the uncoated half (Figure 6d, top right corner). This is also consistent with previous observations, and has been proposed to occur as a result of Al-Mn particles left behind in the corroded regions due to preferential dissolution of the α -Mg phase.⁴² After 18 hours, moderate cathodic currents (average current density of -0.2 A/m^2) were also observed in the wake of the corrosion locations on the PEDOT-coated half (Figure 6e, top left corner). The cathodic current densities detected above these regions were greater in magnitude than those initially observed on the PEDOT-coated half (Figure 6a), demonstrating that the corrosion regions on the PEDOT-coated half also became cathodically activated. After 24 hours, significantly reduced cathodic currents (average current density of -0.08 A/m^2) were observed above the aged corrosion regions, which is again consistent with previous observations.⁴² Upon further examination of Figures 6c,6f, the initially observed electrochemical differences between the PEDOT-coated and uncoated sides of the specimen (Figure 6a) appeared to be eliminated after significant coverage of both sides by the corrosion products. The SEM characterization of the PEDOT-coated AZ31B surface after 22 hours of immersion in 0.01 M NaCl solution shows breakdown of the PEDOT layer and formation

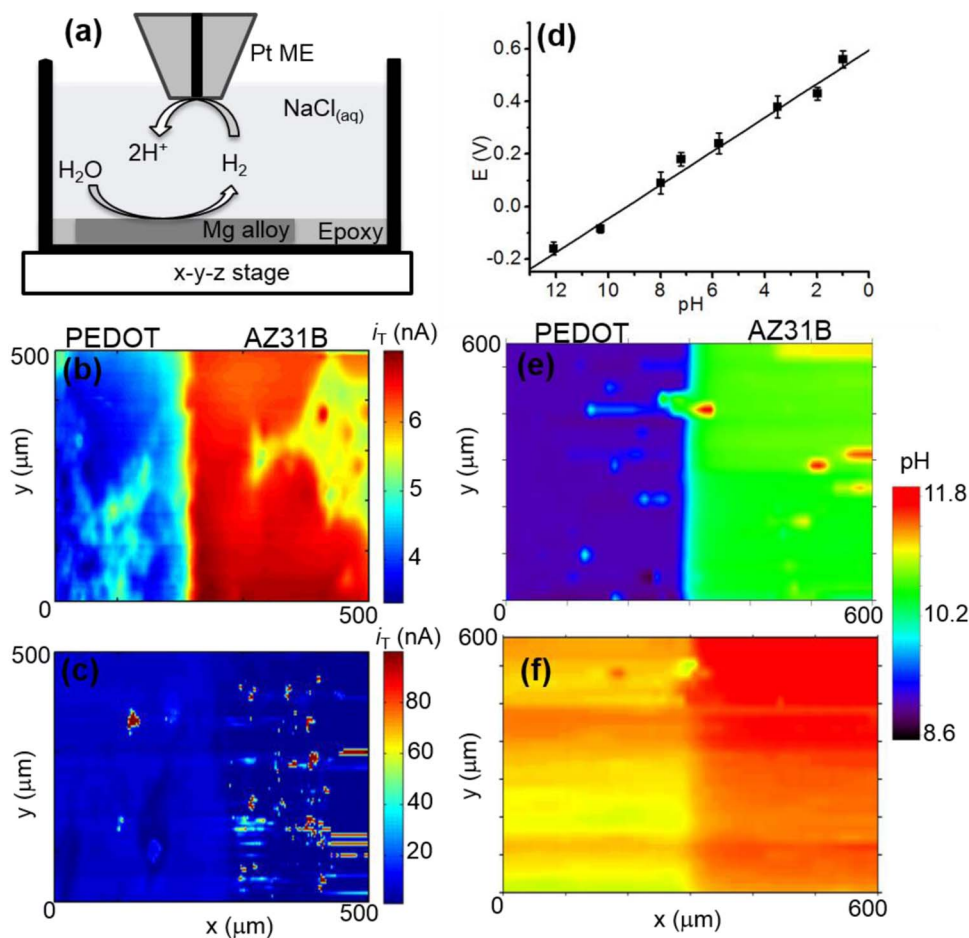


Figure 7. (a) Schematic side view of an amperometric SECM set-up. The maps of SECM tip currents for detection of H_2 evolved at the interface between uncoated and PEDOT-coated AZ31B (b) after 30 minutes and (c) after 24 hours immersion in 0.01 M NaCl aqueous solution. The Pt ME was biased at -0.05 V vs Ag/AgCl-QRE and placed $10\ \mu\text{m}$ from the surface using shear force distance control. The image acquisition required 30 minutes. (d) Calibration curve correlating the open circuit potential of Pt/IrO_x microprobe to the pH of buffer solutions. The pH maps measured with Pt/IrO_x microprobe operated in constant height potentiometric mode of SECM: (e) after 30 minutes and (f) after 24 hours immersion in 0.01 M NaCl.

corrosion products underneath any remaining PEDOT film on the surface (Supporting Information, Figure SI-8c,d).

SECM imaging of local fluxes of H_2 evolution.—To characterize the difference in H_2 evolution fluxes from uncoated and PEDOT-coated AZ31B, the SECM SG/TC mode was employed, as schematically illustrated in Figure 7a. Figure 7b and c shows the SECM maps of H_2 detection currents at Pt ME ($25\ \mu\text{m}$ diameter) for a scan area of $500\ \mu\text{m} \times 500\ \mu\text{m}$ across the interface of uncoated and PEDOT-coated AZ31B surface ((b) after 30 minutes and (c) after 24 hours immersion of the sample in 0.01 M NaCl solution). Under these experimental conditions, the maximum current of H_2 oxidation measured at Pt ME over uncoated AZ31B surface was about 8 nA (after 30 minutes) and 100 nA (after 24 hours), while that of the PEDOT-coated AZ31B is about 3 nA (after 30 minutes) and 20 nA (after 24 hours). Furthermore, the H_2 evolution activities have also been probed by recording Pt ME CVs and approach curves over the isolated uncoated versus PEDOT-AZ31B surfaces (Supporting Information, Figure SI-9 and 10). All these measurements suggested that H_2 being evolved not only from the uncoated AZ31B, but also from the PEDOT-coated AZ31B surface.

After 30 minutes of immersion, higher ME currents for H_2 detection was observed over the uncoated AZ31B side (Figure 7a). This result may seem to contradict with the result of the SVET measurement after 30 minutes of immersion (Figure 6a); however, it should be emphasized here that the local detection of H_2 evolution cannot be directly correlated to local cathodic currents. This is because the rate

of H_2 evolution on Mg-based alloys increases not only as a function of cathodic polarization, but also as a function of anodic polarization (known as the negative difference effect.¹¹) Therefore, the larger ME currents observed on the uncoated AZ31B side after 30 minutes likely reflected the larger anodic currents that were detected with SVET. From the SECM map in Figure 7b, it is possible to notice a heterogeneous ME current mainly on the uncoated side, which was likely associated with the differences in the distribution of intermetallic particles where the H_2 evolution rate is locally different. After 24 hours of immersion, localized regions of intense ME currents (Figure 7c) were detected, which we suspect were reflective of the NDE associated with the intense anodic currents detected by SVET (Figures 6b–6f). This can be explained based on the in situ scan area images recorded during SVET measurements which show the formation of H_2 bubbles from the propagating fronts of the corrosion regions.⁴⁴ Therefore, after 24 hours immersion, the intense ME current observed do not necessarily correspond to Al-Mn particles, but may correspond to anodic peaks that were similarly observed in the SVET measurements. It should also be noted that the SECM measurements generally had better spatial resolution than the SVET measurements, which could explain the discrepancies between the sizes and spatial distribution of the SECM-detected intense ME currents (Figure 7c) compared to the SVET-detected intense anodic currents (Figures 6b–6f). Intense H_2 activity related to active corrosion fronts, appears to be anodic hydrogen.

SECM imaging of local pH distribution.—The pH microprobe fabricated in this work was calibrated using eight buffer solutions ranging from pH 1.02 to 12.10, before and after SECM measurements. A typical open circuit potential versus pH calibration curve for the Pt/IrO_x microprobe is shown in Figure 7d. A slope of -63.4 mV/pH with a correlation coefficient of 0.9886 was obtained for the as-prepared pH microprobe. After performing a series of measurements, recalibration yielded a slope of -63.9 mV/pH with a correlation coefficient of 0.9874. The stable slope of the calibration curve during the course of the experiment allowed direct pH determination from the initial calibration curve.

To map the pH change near the surface of PEDOT-coated AZ31B/bare AZ31B couple during corrosion in 0.01 M NaCl solution, we implemented potentiometric mode of SECM. Prior to adding electrolyte solution, the pH probe was positioned 10 μm above the surface of the sample using shear force distance control mechanism.²⁹ Then the solution was added and the open-circuit potential of the sensor was monitored by laterally scanning the sensor in constant height at a scan speed of 2 $\mu\text{m}/\text{s}$ with a lateral resolution of 20 μm over an area of 600 $\mu\text{m} \times 600 \mu\text{m}$. Figures 7e and 7f show the SECM images of pH profiles near the surface at the interface between uncoated and PEDOT-coated AZ31B after 30 minutes and 24 hours immersion in 0.01 M NaCl solution, respectively. After 30 minutes immersion (Figure 7e), pH measured near uncoated AZ31B were more alkaline than that measured near PEDOT-coated AZ31B with maximum pH values of 9.3 and 8.7, respectively. For the sake of comparison, the pH values in the bulk 0.01 M NaCl solution in the absence and presence of AZ31B alloy substrate were also measured and found to be 6.7 and 8.0, respectively, indicating that average pH value of bulk solution in the presence of AZ31B sample was more alkaline than that measured without the AZ31B electrode. The increase in pH at the corroding AZ31B surface appears to be due to the low solubility of Mg(OH)₂.

After 30 minutes immersion (Figure 7e), resolved cathodic activity of individual intermetallic particles (light blue locations on the pH map) can be observed at the interface on the PEDOT-coated side, which is consistent with the Zn-enrichment found at the uncoated/PEDOT-coated interface by the TEM analysis (see above). On the uncoated AZ31B side, the pH values were relatively uniform across the surface with an average value of 8.7. Resolving the localized activity on the pH maps would depend on the size and distribution of the intermetallic particles, as well as on the size of the pH microprobe. Therefore, the observation of relatively uniform pH (a sea of green region) in the pH map of uncoated AZ31B side implies that the particles were too fine and too closely congregated to be individually resolved by the size of the pH microprobe used. However, there are some locations with more cathodic behavior on the uncoated side (red locations of Figure 7e), perhaps in these locations the intermetallic particles are larger. After 24 hours immersion (Figure 7f), the overall pH value near the uncoated/coated AZ31B interface increased and the pH difference between the PEDOT-coated side and uncoated side is reduced compared to 30 minutes immersion test.

Discussion

Owing to the high reactivity of Mg alloys, a surface adsorbed film can form upon immersion of Mg alloy in RTIL. For example, recently Forsyth et al.¹⁹ reported the formation of up to 100 nm thick surface film upon exposure of pure Mg to an ionic liquid based on bis(trifluoroethylsulfonyl)imide TFSI⁻ anion. In the case of noble metals, the formation of surface adsorbed EDOT layer was also commonly observed (e.g. when Au is in contact with EDOT solution). Hence, prior to electrodeposition, one can expect the formation of multilayered films composed of adsorbed TFSI⁻ anions, EDOT molecules based on thiophene-sulfur interaction with the Mg alloy, and the native oxide/hydroxide films.

During electrodeposition of PEDOT on AZ31B, performed by successive oxidation of 0.1 M EDOT monomer using CV in 0.01 M EMI⁺TFSI⁻ electrolyte solution, the TFSI⁻ anions are generally acknowledged as dopants.⁴⁵ The electropolymerization occurs by way

of two mechanisms: polymer-adsorption and surface-propagation.⁴⁶ The former involves a solution process wherein the polymers and/or oligomers formed in the solution precipitate on the electrode surface,⁴⁷ while the later involves propagation of the polymer on the electrode surface.⁴⁶ The electropolymerization of conducting polymer on Mg alloys electrode is generally thought to proceed through a polymer-adsorption favored mechanism.^{18,36}

The resulting PEDOT containing film is porous based on the SEM results (Figure, SI-9 (a, b)). The elemental analysis from the PEDOT layer shows C, O, F, and S. We also detected Mg and Al-Mn intermetallic particles within the deposited layer. The analysis of TEM-Bright-Field (BF) micrograph in panel (a) of Figure 3, shows that moving away from the base alloy, the size of the pores gradually decreases. This is consistent with the previous report, that postulated the structure or morphology of the PEDOT film contains two types of coexisting zones: a compact and an open structure.⁴⁸ The film can develop tensile stress as it grows, resulting in expansion of the lower layers. The TEM analysis of the bulk of the coating layer further suggests the formation composite film of MgO/Mg(OH)₂ and PEDOT (Figure 4).

To evaluate the corrosion protection conferred by the PEDOT electrodeposited layer, we considered its ability to either anodically protect the Mg alloy or its effective use as a physical barrier layer.⁴⁹ Unlike anodic protection observed in conducting polymer coated stainless steels,⁴⁹ which display a passivation zone upon anodic polarization, PEDOT coated Mg alloys confer a limited corrosion protection due to the barrier effect. Indeed, the PEDOT coating reduces the rate of the anodic and cathodic reactions on AZ31B (shown by the localized PDP curves). The cathodic reaction kinetics also seem to increase on the PEDOT coating as a function of immersion time (shown by localized PDP curves), which may be due to penetration of the electrolyte into the pores of the PEDOT coating, reaching the Al-Mn particles. The pH maps also reflect the level of cathodic activity on each surface, since the cathodic reaction ($2\text{H}_2\text{O} + 2\text{e}^- \rightarrow \text{H}_2 + 2\text{OH}^-$) causes an increase of the local solution pH. Therefore, we can see from the pH maps that the cathodic reaction rate increases on the PEDOT coating as a function of immersion time, since the pH difference between the PEDOT-coated side and uncoated side is reduced after 24 hours.

Although the PEDOT coating reduced the rate of uniform corrosion (demonstrated by the reduction of i_{corr} from the PDP measurements), it did not appear to suppress the propagation of localized corrosion locations. In the SVET measurements, corrosion regions initiated on the uncoated side and spread to the PEDOT-coated side. These results were corroborated by the SECM experiments where the intense H₂ evolution fluxes observed over the PEDOT-coated surface after 24 hours correspond likely to the heads of the propagating corrosion filaments.

Conclusions

A conducting polymer PEDOT coating has been electrodeposited on AZ31B magnesium alloy from ionic liquid by cyclic voltammetry. As a result of ionic liquid as electrolyte, the alloy corrosion during PEDOT electrodeposition is minimized and produces relatively uniform PEDOT coatings. Localized PDP studies of isolated uncoated and coated samples showed the PEDOT coating reduces the rate of the anodic and cathodic reactions on AZ31B. The SVET, amperometric SECM and potentiometric SECM measurements revealed an initial difference between the electrochemical behaviors of the uncoated and PEDOT-coated AZ31B alloy. However, this difference appeared to be nullified after significant coverage by localized corrosion regions. This is because the diffusion of corrosive species (such as Cl⁻) can cause a gradual damage of the passive layer on the AZ31B substrate and subsequent initiation and propagation of localized corrosion will result in the failure of the corrosion protection of the PEDOT coating. This is a valuable study for the community considering the initial interest in PEDOT coating of Mg alloy for use in biomedical implants and potential claims of beneficial passivation.

Acknowledgments

The authors acknowledge funding by General Motors Canada and the Natural Sciences and Engineering Research Council of Canada (NSERC). The electron microscopy observations were carried out at the Canadian Centre for Electron Microscopy, a National Facility supported by NSERC, and McMaster University. Z.P. Cano wishes to acknowledge the Automotive Partnerships Canada (APC) program for funding. We thank Prof. Schougaard for helpful discussion on PEDOT electrodeposition. The technical contribution of N. Payne is also acknowledged.

References

- G. L. Song and A. Atrens, *Adv. Eng. Mater.*, **1**, 11 (1999).
- J. E. Gray and B. Luan, *J. Alloys Compd.*, **336**, 88 (2002).
- X. B. Chen, N. Birbilis, and T. B. Abbott, *Corrosion*, **67**, 1 (2011).
- G.-L. Song, *Prog. Org. Coat.*, **70**, 252 (2011).
- G.-L. Song and M. Liu, *Corros. Sci.*, **62**, 61 (2012).
- E. F. Emley *Principles of magnesium technology*, Pergamon Press: Oxford, New York, 1966.
- K. Z. Chong and T. S. Shih, *Mater. Chem. Phys.*, **80**, 191 (2003).
- D. E. Tallman, G. Spinks, A. Dominis, and G. G. Wallace, *J. Solid State Electrochem.*, **6**, 73 (2002).
- P. P. Deshpande, N. G. Jadhav, V. J. Gelling, and D. Sazou, *J. Coat. Technol. Res.*, **11**, 473 (2014).
- F. Endres, D. MacFarlane, A. Abbott, and A. Editors *Electrodeposition from Ionic Liquids*, Wiley-VCH Verlag GmbH & Co. KGaA, 2008.
- G. S. Frankel, A. Samaniego, and N. Birbilis, *Corros. Sci.*, **70**, 104 (2013).
- N. Birbilis, A. D. King, S. Thomas, G. S. Frankel, and J. R. Scully, *Electrochimica Acta*, **132**, 277 (2014).
- N. Birbilis, P. C. Howlett, D. R. MacFarlane, and M. Forsyth, *Surf. Coat. Technol.*, **201**, 4496 (2007).
- H. Ohno In *Electrochemical Aspects of Ionic Liquids*, John Wiley & Sons, Inc.: 2005, p 1.
- P. G. Pickup and R. A. Osteryoung, *J. Am. Chem. Soc.*, **106**, 2294 (1984).
- W. Lu, A. G. Fadeev, B. Qi, E. Smela, B. R. Mattes, J. Ding, G. M. Spinks, J. Mazurkiewicz, D. Zhou, G. G. Wallace, D. R. MacFarlane, S. A. Forsyth, and M. Forsyth, *Science*, **297**, 983 (2002).
- M. C. Li, C. A. Ma, B. Y. Liu, and Z. M. Jin, *Electrochem. Commun.*, **7**, 209 (2005).
- X. Luo and X. T. Cui, *Acta Biomater.*, **7**, 441 (2011).
- M. Forsyth, P. C. Howlett, S. K. Tan, D. R. MacFarlane, and N. Birbilis, *Electrochem. Solid-State Lett.*, **9**, B52 (2006).
- L. B. Groenendaal, F. Jonas, D. Freitag, H. Pielartzik, and J. R. Reynolds, *Adv. Mater.*, **12**, 481 (2000).
- D. Hohnholz, A. G. MacDiarmid, D. M. Sarno, and W. E. Jones Jr., *Chem. Commun.*, 2444 (2001).
- M. Sebaa, T. Y. Nguyen, S. Dhillion, S. Garcia, and H. Liu, *J. Biomed. Mater. Res., Part A*, **103A**, 25 (2015).
- O. Zubillaga, F. J. Cano, I. Azkarate, I. S. Molchan, G. E. Thompson, and P. Skeldon, *Surf. Coat. Technol.*, **203**, 1494 (2009).
- S. Chaudhari and P. P. Patil, *J. Appl. Polym. Sci.*, **109**, 2546 (2008).
- K. Ogle, V. Baudu, L. Garrigues, and X. Philippe, *J. Electrochem. Soc.*, **147**, 3654 (2000).
- R. M. Souto, B. Normand, H. Takenouti, and M. Keddam, *Electrochim. Acta*, **55**, 4551 (2010).
- J. Izquierdo, J. J. Santana, S. Gonzalez, and R. M. Souto, *Electrochim. Acta*, **55**, 8791 (2010).
- J. J. Santana, J. Gonzalez-Guzman, L. Fernandez-Merida, S. Gonzalez, and R. M. Souto, *Electrochim. Acta*, **55**, 4488 (2010).
- L. Danis, M. E. Snowden, U. M. Tefashe, C. N. Heinemann, and J. Mauzeroll, *Electrochim. Acta*, **136**, 121 (2014).
- S. A. M. Marzouk, *Anal. Chem.*, **75**, 1258 (2003).
- R. P. Buck and E. Lindner, *Pure Appl. Chem.*, **66**, 2527 (1994).
- U. M. Tefashe, M. E. Snowden, P. D. Ducharme, M. Danaie, G. A. Botton, and J. Mauzeroll, *J. Electroanal. Chem.*, **720–721**, 121 (2014).
- M. Danaie, R. M. Asmussen, P. Jakupi, D. W. Shoesmith, and G. A. Botton, *Corros. Sci.*, **83**, 299 (2014).
- G. Williams and H. N. McMurray, *J. Electrochem. Soc.*, **155**, C340 (2008).
- S. Asavapiryanont, G. K. Chandler, G. A. Gunawardena, and D. Pletcher, *J. Electroanal. Chem. Interfacial Electrochem.*, **177**, 229 (1984).
- C. P. Andrieux, P. Audebert, P. Hapiot, and J. M. Saveant, *J. Phys. Chem.*, **95**, 10158 (1991).
- E. M. Genies, G. Bidan, and A. F. Diaz, *J. Electroanal. Chem. Interfacial Electrochem.*, **149**, 101 (1983).
- C. Kvarnström, H. Neugebauer, S. Blomquist, H. J. Ahonen, J. Kankare, A. Ivaska, and N. S. Sariciftci, *Synthetic Metals*, **101**, 66 (1999).
- S. Ahmad, M. Deepa, and S. Singh, *Langmuir*, **23**, 11430 (2007).
- K. A. Unocic, H. H. Elsentriecy, M. P. Brady, H. M. Meyer, G. L. Song, M. Fayek, R. A. Meisner, and B. Davis, *J. Electrochem. Soc.*, **161**, C302 (2014).
- Z. P. Cano, M. Danaie, J. R. Kish, J. R. McDermid, G. A. Botton, and G. Williams, *Corrosion*, **71**, 146 (2015).
- G. Williams, H. ap Llwyd Dafydd, and R. Grace, *Electrochim. Acta*, **109**, 489 (2013).
- J. R. Kish, G. Williams, J. R. McDermid, J. M. Thuss, and C. F. Glover, *J. Electrochem. Soc.*, **161**, C405 (2014).
- G. Williams and R. Grace, *Electrochim. Acta*, **56**, 1894 (2010).
- P. Hapiot and C. Lagrost, *Chem. Rev. (Washington, DC, U. S.)*, **108**, 2238 (2008).
- H. Sakaguchi, H. Matsumura, and H. Gong, *Nat. Mater.*, **3**, 551 (2004).
- D. J. Fermin and B. R. Scharifker, *J. Electroanal. Chem.*, **357**, 273 (1993).
- H. Randriamahazaka, C. Plesse, D. Teyssié, and C. Chevrot, *Electrochem. Commun.*, **5**, 613 (2003).
- J. Fang, K. Xu, L. Zhu, Z. Zhou, and H. Tang, *Corros. Sci.*, **49**, 4232 (2007).